6-22-2007

Asp-120 Locates Zn2 for Optimal Metallo-β-lactamase Activity

Leticia l. Llarrull
University of Notre Dame

Stella M. Fabiane
King's College London

Jason M. Kowalski
Medical College of Wisconsin

Brian Bennett
Marquette University, brian.bennett@marquette.edu

Brian J. Sutton
King's College London

See next page for additional authors

Published version. *Journal of Biological Chemistry*, Vol. 282, No. 25 (June 22, 2007): 18276-18285. DOI.

THE JOURNAL OF BIOLOGICAL CHEMISTRY VOL. 282, NO. 25, pp. 18276–18285, June 22, 2007
Printed in the U.S.A.

Asp-120 Locates Zn2 for Optimal Metallo-β-lactamase Activity*[S]

Received for publication, January, 25, 2007, and in revised form, April 2, 2007 Published, JBC Papers in Press, April 10, 2007, DOI 10.1074/jbc.M700742200

Leticia I. Llarrull[‡1], Stella M. Fabiane[§], Jason M. Kowalski[¶], Brian Bennett[¶2], Brian J. Sutton[§], and Alejandro J. Vila[‡3]

From the [‡]Departamento de Química Biológica-Area Biofísica, Instituto de Biología Molecular y Celular de Rosario, Facultad de Ciencias Bioquímicas y Farmacéuticas, Universidad Nacional de Rosario, Suipacha 531, S2002LRK Rosario, Argentina, [§]Randall Division of Cell and Molecular Biophysics, King's College London, New Hunt's House, Guy's Campus, London Bridge, SE1 1UL London, United Kingdom, and [¶]National Biomedical EPR Center, Department of Biophysics, Medical College of Wisconsin, Milwaukee, Wisconsin 53226-0509

Metallo-β-lactamases are zinc-dependent hydrolases that inactivate β-lactam antibiotics, rendering bacteria resistant to them. Asp-120 is fully conserved in all metallo-β-lactamases and is central to catalysis. Several roles have been proposed for Asp-120, but so far there is no agreed consensus. We generated four site-specifically substituted variants of the enzyme BcII from *Bacillus cereus* as follows: D120N, D120E, D120Q, and D120S. Replacement of Asp-120 by other residues with very different metal ligating capabilities severely impairs the lactamase activity without abolishing metal binding to the mutated site. A kinetic study of these mutants indicates that Asp-120 is not the proton donor, nor does it play an essential role in nucleophilic activation. Spectroscopic and crystallographic analysis of D120S BcII, the least active mutant bearing the weakest metal ligand in the series, reveals that this enzyme is able to accommodate a dinuclear center and that perturbations in the active site are limited to the Zn2 site. It is proposed that the role of Asp-120 is to act as a strong Zn2 ligand, locating this ion optimally for substrate binding, stabilization of the development of a partial negative charge in the β-lactam nitrogen, and protonation of this atom by a zinc-bound water molecule.

β-Lactamases are hydrolytic enzymes produced by bacteria as a mechanism of resistance to β-lactam antibiotics (1, 2). These enzymes are capable of catalyzing the scission of the amide bond of the β-lactam ring characteristic of this class of antibiotics, rendering them ineffective toward their targets. They can be broadly divided into serine-β-lactamases and metallo-β-lactamases, based on their active sites and catalytic mechanisms. β-Lactam hydrolysis takes place by a nucleophilic attack to the carbonyl group, and a subsequent C-N cleavage, usually aided by protonation of the bridging nitrogen atom (3) (Scheme 1).

In the case of serine-β-lactamases, the reaction proceeds through formation of a covalent intermediate with the nucleophilic Ser-70 (4). Based on this mechanistic feature, clinically useful inhibitors for serine-β-lactamases have been designed, such as clavulanic acid and tazobactam, that give rise to irreversible inhibition by formation of a covalent adduct with the enzyme (5). In contrast, MβL[4]-mediated catalysis does not proceed through such an intermediate, thus rendering these inhibitors ineffective (6).

The spread of plasmid-encoded MβL genes among opportunistic and pathogenic bacteria, together with the lack of clinically useful inhibitors, is becoming a serious and yet unsolved clinical problem (7). The elucidation of the catalytic mechanisms employed by MβLs to hydrolyze β-lactam antibiotics is a prerequisite for rational inhibitor design.

The activity of MβLs is dependent on the presence of either one or two Zn(II) ions in their active sites. MβLs have been classified into three subgroups (B1, B2, and B3), based on amino acid sequence similarity, substrate profile, and structural properties (8). The diversity of these subgroups, exemplified by the vastly different efficacies of nonclinical inhibitors toward MβLs, led to the prediction that finding a single inhibitor for all metallo-β-lactamases may not be possible. The search for any common mechanistic feature of MβLs is therefore a high priority.

The first crystal structure solved for an MβL was that of BcII from *Bacillus cereus*, which revealed one Zn(II) ion bound to three His residues (His-116, His-118, and His-196) and a H_2O molecule, in the so-called Zn1 or 3H site (9). Subsequent structures of BcII (10) and other B1 MβLs (11–13) revealed a dinuclear metal center containing the tetrahedral 3H site and an additional trigonal bipyramidal Zn(II) site (the Zn2 or DCH site), where the metal ion is coordinated to Asp-120, Cys-221, His-263, a bridging H_2O/OH^-, and an additional water molecule (Fig. 1). An analogous binding site in B3 enzymes is provided by Asp-120, His-121, and His-263 (DHH site) (14, 15). B2 enzymes, however, are active as mononuclear enzymes, with the only Zn(II) ion located in the DCH site (16). Despite these

* This work was supported in part by grants from Agencia Nacional de Promocion Cientifica y Tecnologica and Howard Hughes Medical Institute (to A. J. V.). The costs of publication of this article were defrayed in part by the payment of page charges. This article must therefore be hereby marked "*advertisement*" in accordance with 18 U.S.C. Section 1734 solely to indicate this fact.

The atomic coordinates and structure factors (code 2UYX) have been deposited in the Protein Data Bank, Research Collaboratory for Structural Bioinformatics, Rutgers University, New Brunswick, NJ (http://www.rcsb.org/).

[S] The on-line version of this article (available at http://www.jbc.org) contains supplemental Figs. S1 and S2 and Refs. 1–3.

[1] Recipient of a doctoral fellowship from Consejo Nacional de Investigaciones Cientificas y Tecnicas.

[2] Supported by National Institutes of Health Grants AI056231 and RR001980.

[3] Staff member from CONICET and an International Research Scholar of the Howard Hughes Medical Institute. To whom correspondence should be addressed. Tel.: 54-341-4350661; Fax: 54-341-4390465; E-mail: vila@ibr.gov.ar.

[4] The abbreviations used are: MβL, metallo-β-lactamase; SKIE, solvent kinetic isotope effect; CT, charge transfer; WT, wild type.

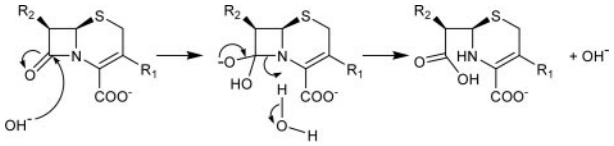

SCHEME 1

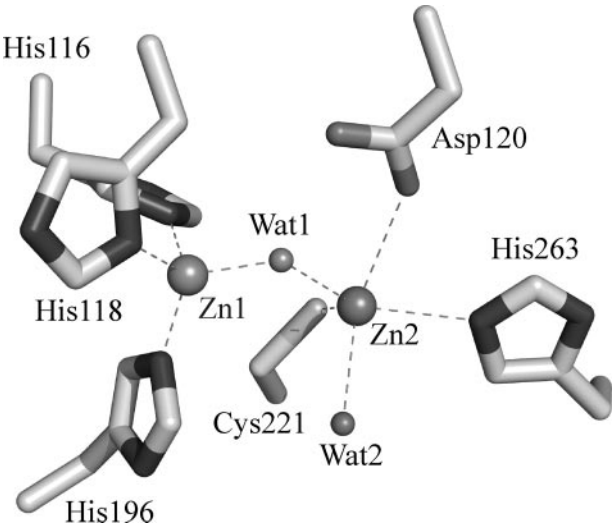

FIGURE 1. **Structure of the active site of wild-type BcII.** The image shows the active site of diZn(II)-BcII according to the crystal structure reported by Fabiane *et al.* (10) (Protein Data Bank code 1bc2) and was generated with Pymol (DeLano Scientific).

differences, Asp-120 is fully conserved in all metallo-β-lactamases identified so far.

Substitution of Asp-120 in B1 and B3 MβLs have shown that this residue is central to catalysis (17–20). The involvement of Asp-120 in catalysis as a nucleophile was initially ruled out by Bounaga *et al.* (21) and Wang *et al.* (22). Since then, the following have been proposed: 1) Asp-120 is the proton donor in the rate-determining step of β-lactam hydrolysis (17, 21, 23); 2) Asp-120 is a general base in the mechanism (21, 24, 25); 3) Asp-120 helps in steering the attacking nucleophile (15, 20, 26); and 4) Asp-120 orients a zinc-bound water molecule that behaves as the proton donor (17, 19, 27, 28).

Despite all the efforts aimed at determining the role of Asp-120 in the hydrolysis of β-lactam antibiotics, there is no agreed consensus. To provide further evidence regarding the role of Asp-120, we generated four site-specifically substituted variants of the enzyme BcII from *B. cereus*. Asp-120 was replaced by an asparagine, a glutamic acid, a glutamine, and a serine to create the BcII mutant proteins D120N, D120E, D120Q, and D120S, respectively. Based on a series of biochemical, spectroscopic, and crystallographic studies, here we propose that the principal role of Asp-120 in MβLs is defining the position of the Zn2 ion, which is crucial for stabilizing the development of a negative charge on the β-lactam nitrogen atom, providing the water molecule that protonates this nitrogen, and binding the substrate.

EXPERIMENTAL PROCEDURES

Reagents

All chemicals were of the highest quality available. *Escherichia coli* BL21(DE3)pLysS′ cells (Stratagene, CA) were employed for protein production. *E. coli* JM109 cells (Stratagene, CA) were employed for transformation with plasmid DNA and ligation mixtures. Luria-Bertani medium (Sigma) was used as growth media for all bacterial strains.

DNA Techniques

DNA preparation and related techniques were performed according to standard protocols (29). Plasmid DNA was isolated using the Wizard Plus SV minipreps kit (Promega). DNA was extracted from agarose gels using QIAEX II kit (Qiagen) or GFX columns (Amersham Biosciences).

Site-directed Mutagenesis

A preparation of pETβLII plasmid DNA (30) was digested with BamHI and PstI and subcloned into a vector pBluescript II KS(−) previously digested with the same restriction endonucleases, to obtain the plasmid KS-NH_3, which contains the DNA fragment coding for the NH_3-terminal half of BcII (31). This plasmid was used as the DNA template for the PCR-based mutagenesis protocol. Site-directed mutagenesis was performed using the *megaprimer* PCR protocol (32). The first PCR was carried out using the plasmid KS-NH_3 as the template DNA, the *ks-reverse* primer (5′-TCACACAggAAACAgCTATgAC-3′), and the corresponding mutagenic primer: D120_N_SphI (5′-CACATgCgCA**T**gCT***A***ATCgAATTggCgg-3′) for D120N, D120_S_SphI (5′-CACATgCgCA**T**gCT***Ag***TCgAATTggCgg-3′) for D120S, D120_E_SphI (5′-CACATgCgCA**T**gCTgA***A***CgAATTggCgg-3′) for D120E, and D120_Q_SphI (5′-CACATgCgCA**T**gCT***C***A***A***CgAATTggCgg-3′) for D120Q. The mutagenic primers were designed to introduce a recognition site for the restriction endonuclease SphI, through the introduction of a silent mutation, using the software Primer Tailoring (33). Boldface underlined letters indicate the silent mutation, and boldface italic underlined letters indicate the nonsilent mutations. A 100-μl reaction mixture, containing 0.2 mM of each dNTP, 0.5 pmol/μl of each primer, 1 mM $MgSO_4$, 100 ng of template DNA (KS-NH_3), 10 μl of the 10× buffer provided with the polymerase (New England Biolabs), and 2 units of *Vent* DNA polymerase (New England Biolabs), was used in the PCR, using a GeneAmp® PCR System 2400 equipment (PerkinElmer Life Sciences). The following cycles were employed in the first PCR: 1) 1 cycle of 3 min at 94 °C; 2) pause for the addition of the DNA polymerase; 3) 30 cycles of 2 min at 94 °C, 3 min at 48 °C, and 2 min at 72 °C; and 4) 1 cycle of 3 min at 72 °C. The PCR mixture was resolved in a 2% agarose gel containing ethidium bromide, and the 210-bp PCR product (the *megaprimer*) was recovered from the excised agarose fragment using the QIAEX II kit (Qiagen). The second PCR was carried out using the same template DNA, the megaprimer that codes for the desired mutation, and the ks-forward primer (5′-CgCCAgggTTTTCCCAgTCACgAC-3′). All the megaprimer recovered from the first PCR was used in the second round of amplification, in a 50-μl reaction mixture, containing 0.2 mM of each dNTP, 0.5 pmol/μl of the ks-forward primer, 1 mM $MgSO_4$, 100 ng of template DNA (KS-NH_3), 5 μl of the 10× buffer provided with the polymerase (New England Biolabs Inc.), and 1.2 units of *Vent* DNA polymerase (New England Biolabs Inc.). The following cycles were employed in the second

PCR: 1) 1 cycle of 5 min at 94 °C; 2) pause for the addition of the DNA polymerase; 3) 35 cycles of 2 min at 94 °C, 2 min at 55 °C, and 2 min at 72 °C; and 4) 1 cycle of 4 min at 72 °C. The amplification was corroborated by gel electrophoresis, and the 579-bp purified PCR product was digested with the restriction endonucleases BamHI and PstI and cloned into pBluescript II KS(−), previously digested with the same endonucleases. After transformation of *E. coli* JM109 cells with the ligation mixture, the presence of the mutated DNA sequences in the plasmid DNA preparations from selected clones was first corroborated by digestion of the DNA with the restriction endonuclease SphI, whose recognition site was introduced by the mutagenic primers. Afterward, the sequences were confirmed by DNA sequencing (University of Maine Sequencing Facility). The genes that code for the Asp-120 mutants of the metallo-β-lactamase BcII were reconstructed by cloning the DNA fragment coding for the mutagenized NH_3-half of BcII, digested with the enzymes BamHI and PstI, and the DNA fragment coding for the wild-type COOH-half of BcII, digested with PstI and HindIII, into the plasmid pET-TERM (31) previously digested with the restriction endonucleases BamHI and HindIII. The expression vector pET-TERM allows expression of the protein of interest as an amino-terminal fusion to the enzyme glutathione *S*-transferase from *Schistosoma japonicum*, under control of the T7 promoter, and presents the termination sequence from the *BcII* gene. The DNA fragment that codes for the COOH-terminal half of BcII was purified, after digestion with PstI and HindIII, from the plasmid KS-CT_2 (31).

Enzyme Purification

Wild-type BcII and Asp-120 mutants were expressed in *E. coli* BL21(DE3)pLysS′ cells as fusion proteins with glutathione *S*-transferase, purified, and quantified as follows. Typically, the cell pellet obtained from 50 ml of a saturated culture in LB medium, supplemented with 150 μg/ml ampicillin and 35 μg/ml chloramphenicol, was resuspended in fresh medium and used to inoculate 1-liter of LB medium supplemented with 150 μg/ml ampicillin and 35 μg/ml chloramphenicol, in a 5-liter Erlenmeyer flask. Cells were grown for 2 h at 37 °C until the A_{600} = 1 was reached. The expression of fusion protein was induced by addition of 10 g of lactose, and the culture was further incubated at 37 °C for an additional 4-h period. All subsequent purification steps were performed at 4 °C. *E. coli* cells were lysed by sonication in lysis buffer (16 mM Na_2HPO_4, 4 mM NaH_2PO_4, and 150 mM NaCl, pH 7, with 3.3 μg/ml DNase, 5 mM $MgCl_2$, and 1 mM phenylmethylsulfonyl fluoride), and cell debris was separated by ultracentrifugation. The GST-BcII fusion protein was purified by affinity chromatography using a glutathione-Sepharose resin (Amersham Biosciences) as reported previously (30). The pure fractions were treated with bovine plasma thrombin (Sigma) at a 1:100 ratio in 150 mM NaCl, 2.5 mM $CaCl_2$ at 26 °C during 2 h. BcII was purified from the proteolysis mixture by ion-exchange chromatography on Sephadex CM-50 (Amersham Biosciences) as reported previously (30). Protein samples were dialyzed against >100 volumes of 10 mM HEPES, pH 7.5, 0.2 M NaCl. Purity of the enzyme preparations was checked by SDS-PAGE. Protein concentration was measured spectrophotometrically using ϵ_{280} = 30,500 $M^{-1}\cdot cm^{-1}$ (34).

Determination of the Zn(II) Content of the Enzymes

The metal content in the samples of wild-type BcII and Asp-120 mutants was determined under denaturing conditions using the colorimetric metal chelator 4-(2-pyridylazo)resorcinol, as described by Fast *et al.* (35).

Steady-state Kinetic Assays

The kinetic parameters for the hydrolysis of different β-lactam antibiotics catalyzed by wild-type BcII and Asp-120 mutants under steady-state conditions were obtained by determination of the initial rate of reaction at different substrate concentrations. Substrate concentrations were calculated based on the following molar absorptivities: penicillin G, $\Delta\epsilon_{235} = -775\ M^{-1}\cdot cm^{-1}$; cefotaxime, $\Delta\epsilon_{260} = -7{,}500\ M^{-1}\cdot cm^{-1}$; nitrocefin, $\Delta\epsilon_{485} = 17{,}420\ M^{-1}\cdot cm^{-1}$; imipenem, $\Delta\epsilon_{300} = -9{,}000\ M^{-1}\cdot cm^{-1}$. The plots of the dependence of the initial rates on substrate concentration were fitted to the Michaelis and Menten equation, using SigmaPlot 8.0. Reactions were carried out in 10 mM HEPES, pH 7.5, 200 mM NaCl, 20 μM $ZnSO_4$, and 0.05 mg/ml bovine serum albumin at 30 °C. Absorbance changes upon substrate hydrolysis were measured in a Jasco V-550 spectrophotometer, and the temperature was kept constant by means of a Polyscience digital circulator connected to the cell holder in the spectrophotometer.

Solvent Kinetic Isotope Effect Assays

The kinetic parameters obtained for the hydrolysis of different β-lactam antibiotics catalyzed by wild-type BcII and Asp-120 mutants in H_2O, under steady-state conditions, were compared with the kinetic parameters obtained for the same reaction carried out in D_2O. The initial rate of hydrolysis at different substrate concentrations was measured in 10 mM HEPES, pD 7.5 (pH 7.1), 200 mM NaCl, 20 μM $ZnSO_4$, and 0.05 mg/ml bovine serum albumin at 30 °C. The dependence of the initial rates on substrate concentration was fitted to the Michaelis-Menten equation, using SigmaPlot 8.0. The deuterated reaction medium was kept at 30 °C under a N_2 gas atmosphere, prior to reaction. The hydrolysis of the antibiotics was registered in open cells, during less than 5 min, to avoid a significant water uptake from the environment.

Preparation of Metal-free Enzymes

All buffer solutions used to prepare the apoenzymes were treated by extensive stirring with Chelex 100 (Sigma). Apoprotein samples were prepared by dialysis of the purified holoprotein (~200 μM) against two changes of >100 volumes of 10 mM HEPES, pH 7.5, 0.2 M NaCl, 20 mM EDTA over a 12-h period under stirring (36). EDTA was removed from the resulting apoenzyme solution by three dialysis steps against >100 volumes of 10 mM HEPES, pH 7.5, 1 M NaCl, Chelex 100, and three dialysis steps against >100 volumes of 10 mM HEPES, pH 7.5, 0.2 M NaCl, Chelex 100 (36). For the preparation of apoprotein samples used in EPR experiments, the three last dialysis steps were replaced by one dialysis step against >100 volumes of 10 mM HEPES, pH 7.5, 0.2 M NaCl, Chelex 100 and finally two

dialysis steps against >100 volumes of 100 mM HEPES, pH 7.5, 0.2 M NaCl, Chelex 100. All dialysis steps were carried out at 4 °C.

Electronic Spectroscopy of Co(II)-BcII Derivatives

A solution of 200–300 μM apoprotein in 10 mM HEPES, pH 7.5, 0.2 M NaCl was titrated with a 10.6 mM $CoSO_4$ stock solution prepared in 10 mM HEPES, pH 7.5, 0.2 M NaCl. For the UV-visible titration, which was done in parallel with the EPR titration, a solution of 1.2 mM apo-BcII D120S in 100 mM HEPES, pH 7.5, 0.2 M NaCl was titrated with a 6 mM $CoSO_4$ stock solution prepared in 100 mM HEPES, pH 7.5, 0.2 M NaCl. The equivalents of bound Co(II) were calculated as the ratio between the concentration of Co(II) in the sample and the concentration of protein capable of binding metal, which was calculated by multiplying the concentration of protein determined by absorbance at 280 nm by the factor $n/2$, where n is the Zn(II) content of the purified proteins. The spectra were recorded at room temperature in a UV-visible Jasco V-550 spectrophotometer, and difference spectra were obtained by subtracting the spectrum of the corresponding apoprotein.

EPR Spectroscopy

EPR spectroscopy was performed at 13 K, 2 milliwatts, and 9.63 GHz ($B_{microwave} \perp B_{static}$) using a Bruker Elexsys E500 spectrometer equipped with an ER 4116 DM TE_{012}/TE_{102} dual mode X-band cavity and an Oxford Instruments ESR-900 helium flow cryostat.

The apoprotein (1.2 mM), in 100 mM HEPES, pH 7.5, 0.2 M NaCl, was titrated stepwise with a 6 mM $CoSO_4$ stock solution prepared in the same buffer. The Co(II)-containing solution was rapidly mixed with the sample in the EPR tube by manual flicking (37) and frozen in liquid nitrogen. EPR samples for successive additions of Co(II) were quickly thawed (~5 s) from 77 to 293 K by agitating the sample tube in water.

X-ray Crystallography

Crystallization and Data Collection—D120S was crystallized using the vapor diffusion method. 1 μl of the protein solution, at 4.7 mg/ml, was mixed with 1 μl of reservoir solution, containing 17–19% PEG-3350, 0.1 M sodium cacodylate, pH 5.0–5.5, 0.1 M sodium tartrate. Large single crystals grew within a few weeks. These were transferred to a solution supplemented with 25% glycerol and cryocooled by plunging them into liquid nitrogen. The crystals diffract to 1.95 Å resolution, and a data set was collected at CCLRC Daresbury Synchrotron Radiation Source, station 14.2, at a wavelength of 0.9853Å. The space group was C2, with unit cell parameters a = 53.39 Å, b = 61.97Å, c = 69.57Å, and β = 93.28°. The data were reduced and scaled using MOSFLM (38) and SCALA as implemented in the CCP4 package (39). Data processing statistics are given on Table 2. 5% of the reflections, chosen randomly, were assigned for the R_{free} calculations.

Structure Determination and Refinement—The structure was determined by molecular replacement using CNS (40). The crystal structure of the wild-type BcII (Protein Data Bank code 3BC2) was used as a search model, stripped of all noncovalently bound atoms. One clear solution was found, and rigid body refinement yielded R-factor of 30.9% and R_{free} was 31.6%. The structure was refined using CNS during two rounds, and finished using Refmac5 from the CCP4 package. Model building was performed using Quanta (Accelrys) and Coot (41). The TLS groups were chosen using TLSMD (42), run from the TLSMD server (43). The final R_{free} was 22.1%, R-factor for 95% of reflections was 14.6%. It was clear that some of the noncovalently bound atoms (including the Zn(II) ion in position Zn2) were not fully occupied. At 1.95 Å resolution, it was not possible to refine their occupancy and temperature factor simultaneously, and so their occupancies were fixed at 0.5. The final model contains 218 residues, two zinc ions, four glycerol molecules, and 283 waters. Asp-84, as is the case in other structures of the same protein, is in the disallowed region of the Ramachandran plot. The geometry of the model is good as checked by SFCHECK (44), PROCHECK (45), MolProbity (46), and Coot (41).

RESULTS

Biochemical and Enzymatic Characterization of BcII Asp-120 Mutants—To probe the role of Asp-120 in MβLs, we designed the following point mutants: D120S, D120N, D120E, and D120Q. Asparagine was chosen as a chemically distinct but structurally similar substitute for aspartic acid. Glutamic acid was chosen as a chemically similar but structurally distinct surrogate for aspartic acid, and glutamine was chosen for comparison with the D120E mutant and to facilitate correlation with the differences found between WT BcII and D120N. Replacement of aspartic acid with serine was intended to remove both the ability of the residue at this position to bind metal and to interact with the bridging H_2O/OH^-.

The BcII mutants on Asp-120 were expressed in *E. coli* BL21(DE3)pLysS′ as fusion proteins with GST; the fusion proteins were digested with thrombin, and the BcII variants were then purified to homogeneity from the digestion mixture. In all cases, the mutant enzymes were properly folded, as revealed by the CD spectra that were similar to those of WT BcII (data not shown). Thus, major changes in the enzyme activity can be attributed to a direct effect of the introduced mutations on catalysis because the structural integrity of the mutant enzymes is mostly preserved.

The total Zn(II) content was determined by a spectrophotometric assay of the colorimetric reagent 4-(2-pyridylazo)resorcinol, after dialysis of the mutant proteins against a metal-free buffer solution. The measured metal contents were 1.7 Zn(II)/enzyme (WT BcII), 1.2 Zn(II)/enzyme (D120E BcII), 1.9 Zn(II)/enzyme (D120N BcII), 1.6 Zn(II)/enzyme (D120Q BcII), and 1.7 Zn(II)/enzyme (D120S BcII). This suggests that replacement of the conserved metal ligand Asp-120 by a Ser, Asn, Glu, or Gln (with quite different metal ligating capabilities) does not abolish metal binding to the DCH site.

The hydrolytic capabilities of all the purified mutants were tested against different β-lactam substrates under steady-state conditions in the presence of 20 μM added Zn(II), to ensure formation of a dinuclear site. All the four mutants were clearly less active than WT BcII (Table 1). In general, the mutants displayed an impaired affinity toward all substrates, as inferred from the higher K_m values, except for the D120E and D120Q

TABLE 1

Steady-state kinetic parameters for WT BcII and Asp-120 BcII mutants with different substrates and SKIE for nitrocefin and cefotaxime hydrolysis

Reactions were carried out in 10 mM HEPES, pH or pD 7.5, 200 mM NaCl, 20 μM $ZnSO_4$, and 0.05 mg/ml bovine serum albumin at 30 °C. Standard deviation values were <10%.

	Nitrocefin				Imipenem		
	k_{cat}	K_m	k_{cat}/K_m	$^{D}k_{cat}$	k_{cat}	K_m	k_{cat}/K_m
	s^{-1}	μM	$M^{-1}\cdot s^{-1}$		s^{-1}	μM	$M^{-1}\cdot s^{-1}$
WT	7.9	5.7	1.4×10^6	1.41	114	660	1.7×10^5
D120E	3.6	174	2.1×10^4	1.3	35.7	447	8.0×10^4
D120N	5.4	180	2.97×10^4	2.5	14.7	6800	2.2×10^3
D120Q	0.68	922	7.4×10^2	1.26	2.89	142	2.04×10^4
D120S	9×10^{-3}	62	1.5×10^2	1.12	4.7	5100	9×10^2
	Cefotaxime				**Penicillin G**		
	k_{cat}	K_m	k_{cat}/K_m	$^{D}k_{cat}$	k_{cat}	K_m	k_{cat}/K_m
	s^{-1}	μM	$M^{-1}\cdot s^{-1}$		s^{-1}	μM	$M^{-1}\cdot s^{-1}$
WT	67	42	1.6×10^6	1.6	262	509	5.1×10^5
D120E	14.5	97	1.49×10^5	1.33	16.1	1550	1.04×10^4
D120N	5.5	123	4.5×10^4	2.5	9.9	1900	5.2×10^3
D120Q	1.91	270	7.1×10^3	1.49	75	6770	1.1×10^4
D120S	0.176	600	2.9×10^2	1.8	0.41	2700	1.5×10^2

mutants that showed similar and smaller K_m against imipenem compared with WT BcII, respectively.

Among all the studied mutants, BcII D120S showed the poorest catalytic efficiency toward all substrates, with k_{cat}/K_m values lower by between 3 and 4 orders of magnitude compared with the native enzyme. This was mostly because of very low k_{cat} values in this mutant.

BcII D120E was, in general, the most active mutant in the series. Exceptions were BcII D120N with nitrocefin and D120Q with penicillin G, which showed similar activities to D120E with these substrates. BcII D120N and D120Q displayed an intermediate level of activity, with different trends depending on the analyzed substrate. For example, D120N was more active toward nitrocefin and cefotaxime than BcII D120Q, whereas the latter was a better imipenemase and penicillinase than D120N. Interestingly, D120Q showed the smallest k_{cat} value for imipenem hydrolysis and a relatively high binding affinity toward this substrate.

Solvent Kinetic Isotope Effect—The solvent kinetic isotope effect ($^{D}k_{cat}$) was studied for WT BcII and for all the mutants by determining the steady-state catalytic parameters in H_2O and D_2O for nitrocefin and cefotaxime (Table 1). When the reactions were performed with 20 μM added Zn(II), WT BcII showed a normal SKIE ($^{D}k_{cat} > 1$), indicating that the rate-limiting step involves a proton transfer. All BcII D120*X* mutants also presented a normal SKIE. It is interesting to note that this held for BcII D120S, D120N, and D120Q, all mutants lacking a carboxylate moiety in position 120.

Spectroscopic Characterization of the Co(II)-D120X BcII derivatives—To better analyze the metal binding capabilities of the different mutants and to gain some structural insight, we obtained the Co(II) derivatives. The UV-visible spectra of these derivatives obtained upon addition of excess Co(II) to the corresponding mutant apoenzymes are shown in Fig. 2 and compared with the already reported spectrum of Co(II)-substituted WT BcII. All of them show an intense feature in the UV range and a four-pattern band in the visible spectrum, with some minor variations in their intensities and wavelengths. The UV absorption can be attributed, as in the native enzyme, to a Cys-Co(II) charge transfer band arising from Cys-221 bound to

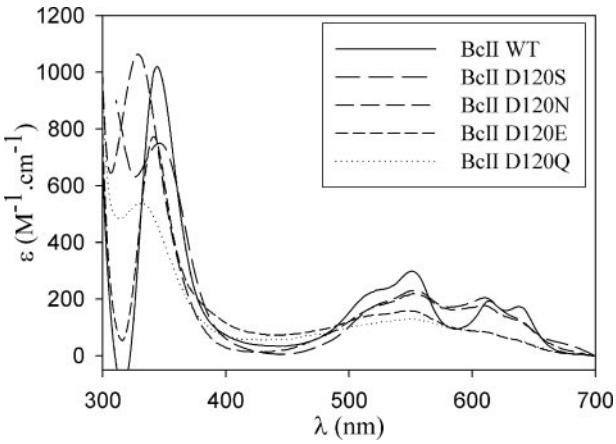

FIGURE 2. **UV-visible spectra of Co(II)-substituted WT BcII and Asp-120 BcII mutants.** The spectra correspond to the di-Co(II) forms in 10 mM HEPES, pH 7.5, 200 mM NaCl. The extinction coefficients were calculated by considering the amount of enzyme determined from the intensity at 280 nm.

Co(II) ion in the DCH site. The finding of this band in all mutants clearly reveals that Co(II) binds at the Cys-221-containing site (which we continue to denote the "DCH" site) despite the substitution of Asp-120. The Cys-Co(II) CT band is found at 330 nm in D120N and D120Q, whereas in WT BcII, D120E, and D120S, the absorption is located at around 343 nm. These changes reveal different levels of (minor) perturbation of the Cys-Co(II) interaction among the different mutants.

The four absorption bands in the visible range correspond to Laporte forbidden *d-d* (or ligand field) electronic transitions of the Co(II) ion bound to the 3H site. A closer inspection of these features reveals different relative intensities of these bands compared with Co(II)-substituted WT BcII. This can be attributed to some distortion of the nominally tetrahedral 3H site or to the presence of an additional absorption in this region arising from the DCH site, induced by the mutation.

When all four mutant apoenzymes were titrated with increasing Co(II) concentrations, the CT and the ligand field bands grew almost simultaneously (as observed in the native enzyme), revealing that both sites are being filled at the same

time under these conditions (data not shown). Although these experimental conditions do not allow us to retrieve reliable dissociation constants, the titration curves clearly show that metal binding is weaker in the mutants than in WT BcII.

An EPR spectrometric titration of the least active BcII variant, D120S, was carried out, and the results are presented in Fig. 3*A*. A UV-visible titration in similar conditions (1 mM concentration) revealed the formation of a Co(II)-D120S BcII species that had not been found when working at lower protein concentrations. In the range of 0.11–0.41 Co(II)/protein ratios, a species with no detectable CT band and a *d-d* pattern different from the one present in the final adduct is detected (supplemental Fig. S1). A CT band at 343 nm is noticeable from 0.97 Co(II) equivalents onwards, which grows steadily until a 2:1 metal ion/protein ratio is achieved.

When the Co(II)-substituted samples were interrogated by EPR spectroscopy, a complex multicomponent EPR signal was observed at low (0.06–0.23 eq) levels of Co(II). This signal strongly resembled that from the B2 lactamase ImiS (47), and contained a saturation-resistant component (supplemental Fig. S2). This signal can be attributed to a highly strained rhombic $M_S = |\pm ½\rangle$ system because of distorted five-coordinate Co(II), as observed in the metallohydrolases DapE (48) and VanX (49), perhaps with water occupying otherwise vacant coordination sites. Based on the absence of a CT band in the UV-visible spectra under these conditions, it follows that this species corresponds to a partially filled 3H site with a distorted pentacoordinated geometry.

Beyond 0.23 eq of Co(II), the BcII saturation-resistant signal ceased to increase in intensity, and a new signal (termed "Axial") was elicited, which appeared to grow linearly with added Co(II) until 1 eq of Co(II). This signal ceased to increase in intensity beyond 1 eq of Co(II), and further additions of Co(II) elicited a third signal, indistinguishable from that of Co(II) in buffer. A plot (Fig. 3*B*) of the total spin density during the EPR titration *versus* the Co(II) equivalents added reveals a steady growth until the addition of ~1 Co(II) equivalent. Then the spin density is almost constant when the Co(II)/BcII ratio is between 1 and 1.8, suggesting the accumulation of an EPR-silent species. This accumulation coincided with the steady disappearance of the BcII axial signal between 1.04 and 1.82 eq of Co(II), with the balance of the spectral density made up of residual BcII saturation-resistant signal and the signal from "free" Co(II). Beyond 2 eq of Co(II), the only change in the spectrum upon addition of Co(II) is increased intensity because of free Co(II). The simplest explanation of these phenomena is the formation of a dinuclear center upon the addition of between 1 and 2 eq of Co(II), with only the $S = 0$ state significantly populated. Thus, EPR data provide a direct evidence of the formation of a di-Co(II) site in D120S BcII.

Structural Characterization of D120S BcII—We obtained crystals of D120S BcII that diffracted to 1.95 Å. The overall structure in the mutant is preserved compared with the WT protein, with the characteristic $\alpha\beta/\beta\alpha$ fold of all MβLs. B1 MβLs are characterized by a mobile loop spanning residues 59–66. No electron density could be traced for this loop in this mutant, suggesting that the mobile features are preserved. Data processing statistics are summarized in Table 2.

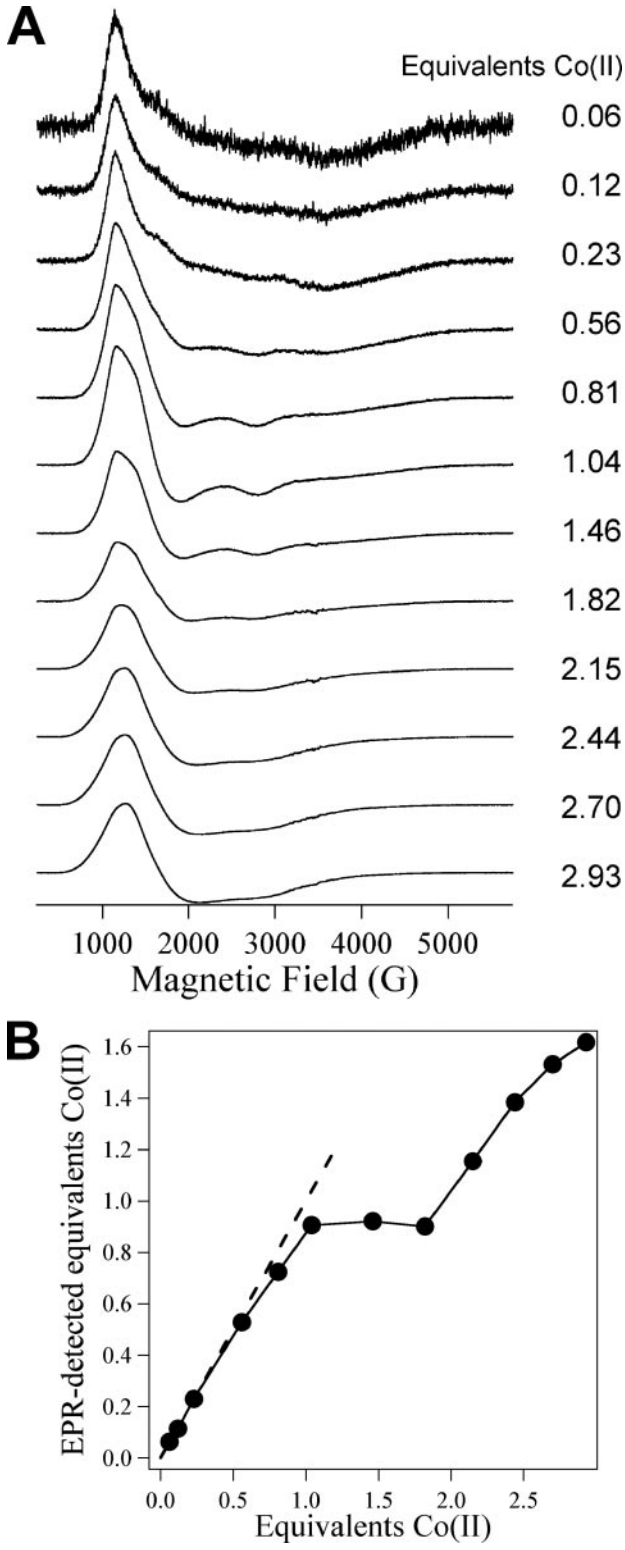

FIGURE 3. **EPR titration of apo-D120S BcII with Co(II).** *A,* X-band EPR titration of apo-D120S BcII with Co(II). Intensities are shown normalized for Co(II) concentration. *B,* EPR-detected Co(II) (*solid circles*) was quantified by double integration of EPR spectra with respect to Co(II) in 50% 10 mM HEPES buffer, pH 7.5, 50% glycerol. The *dashed line* corresponds to the expected behavior where all added Co(II) is EPR-detectable.

The active site of D120S BcII shows two bound Zn(II) ions, resembling the dinuclear site found in the native enzyme (Fig. 4*A*). One of the Zn(II) ions is bound to His-116, His-118, His-

TABLE 2
Crystallographic data collection and refinement statistics

Diffraction data	
Resolution (Å)	1.95
Unit cell	$a = 53.39$ Å, $b = 61.97$ Å, $c = 69.57$ Å, $\beta = 93.28°$
No. of unique reflections	16,580
Completeness (%) (2.00 to 1.95 Å)	99.9 (99.9)
R_{merge} (%)	7.5 (31.7)
$I/\sigma(I)$	7.6 (2.3)
Refinement	
Resolution limits (Å)	31.0 to 1.95
R (%, 95% reflections)	14.6
R_{free} (%, 5% reflections)	22.1
Deviations	
Bond lengths (Å)	0.013
Bond angles (°)	1.366
Mean B factors	
Main-chain atoms (Å^2)	25.44
Side-chain atoms (Å^2)	26.98
Zinc atoms (Å^2)	22.02
Hetero atoms (Å^2)	19.47
Water atoms (Å^2)	37.27
Ramachandran plot	
Favored (%, number)	92.6, 176
Additional allowed (%, number)	6.8, 13
Generously allowed (%, number)	0, 0
Disallowed (%, number)	0.5, 1

196, and a solvent molecule (at a distance of 2.24 Å), in the canonical 3H site. The second Zn(II) is located in a position similar to that in the DCH site of WT BcII. This metal ion clearly had an occupancy lower than 100%, but because of the limited resolution of the data, it was not possible to refine its occupancy and temperature factor simultaneously. With occupancy fixed at 0.5, the temperature factor refined to a value close to those of the surrounding protein ligand atoms. Confirmation that Zn2 indeed has lower occupancy, rather than a high temperature factor, comes from the observation of residual positive electron density for His-263, at a position that in other WT BcII data sets and mutants is associated with the absence of Zn2 (see for example Ref. 50).

Although the Zn2 ligands Cys-221 and His-263 superimpose very well, the position of the Zn2 ion itself is shifted by ~1 Å compared with the DCH site in the WT enzyme (Fig. 4*B*), resulting in a longer zinc-zinc distance (4.24 Å compared with 3.8 Å). Cys-221 and His-263 bind to Zn(II) with typical bond distances (2.21 and 2.09 Å, respectively), whereas the engineered residue Ser-120 is oriented in a similar position as Asp-120 in WT BcII, but it is not able to bind the metal ion, its oxygen atom being at 4.71 Å from the metal ion. Instead, a new water molecule (Wat-*X*) becomes a zinc ligand (Zn–O distance, 2.20 Å). This solvent molecule forms a hydrogen bond with Ser-120, which thus becomes a second shell ligand of the engineered metal site (Fig. 4*A*). A second water molecule is bound to Zn2 at 2.33 Å in a similar position to the Wat-2 ligand in the native enzyme. The coordination geometry of the Zn2 site is thus distorted compared with that of WT BcII.

Other important residues in the hydrogen bond network of the BcII active site are Arg-121 and Lys-224. Arg-121 maintains the same position as in WT BcII, conserving all the H-bonding interactions present in the native enzyme (Asp-84, Ser-69, and Gly-262), except that with Asp-120. The guanidinium group of Arg-121 is far from the OH moiety of Ser-120 in the mutant, but instead forms an H-bond with Wat-*X*, the new Zn2 ligand (Fig. 4*A*). Lys-224 has been refined to two possible conformations with 50% occupancy. In both of them, compared with WT BcII, its amino group is able to directly interact with the second water ligand of Zn2 (Wat-2).

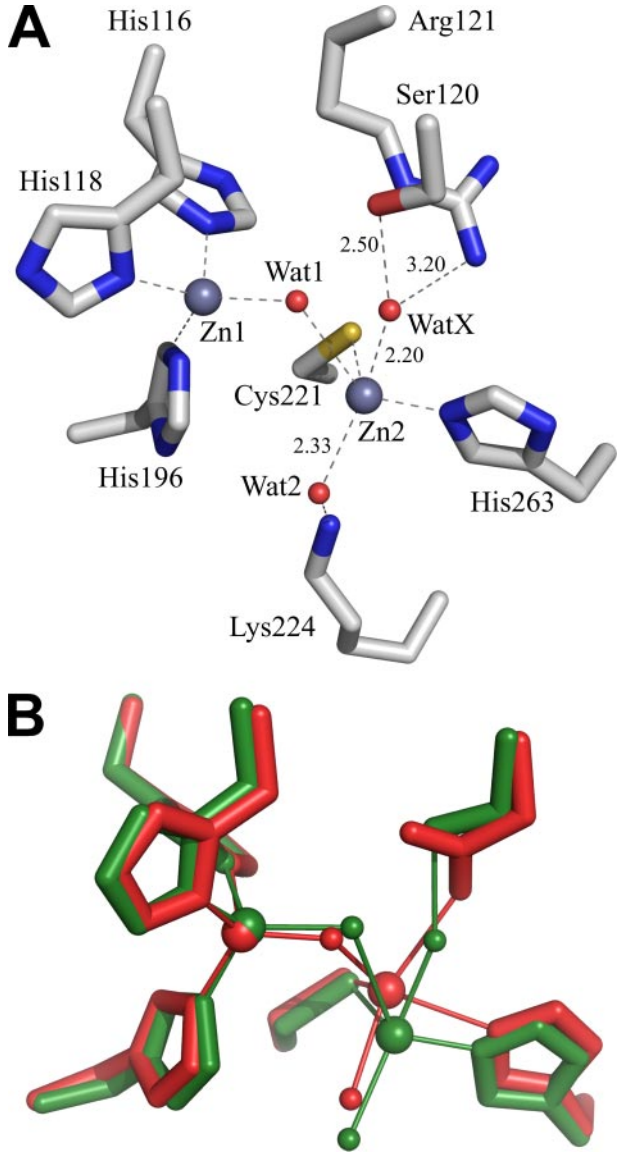

FIGURE 4. **Structure of the active site of D120S BcII.** *A*, active site of D120S BcII, including the metal ligands and key residues in the active site. *B*, comparison of the active sites of D120S (*green*) and WT BcII (*red*). The *larger spheres* represent Zn(II) ions, and the *smaller spheres* represent water molecules.

DISCUSSION

Asp-120 is fully conserved in all MβLs, despite the structural and functional diversity among the different enzymes belonging to this family. Mutagenesis studies on B1 (BcII, CcrA, and IMP-1) and B3 enzymes (L1) have already shown that substitution of Asp-120 by other residues gives rise to poorly active enzymes (18–20, 51). Theoretical studies on B1 and B2 enzymes have also suggested a central role of Asp-120 in catalysis (23, 25, 27, 28, 52). However, the precise role of this residue is still matter of debate. In this work we have performed an enzymatic characterization of four point mutants of the MβL BcII at position 120. We have also studied the Co(II) derivatives

of these mutants and solved the crystal structure of the least active mutant D120S.

All mutants in the position 120 show diminished lactamase capabilities compared with WT BcII. Despite differences depending on the particular substrate, the general activity trend is WT > D120E > D120N ≈ D120Q ≫ D120S. D120E is 2–70 times less active than the native enzyme, whereas D120N is 30–100 times less active than WT BcII. The activity of D120Q is decreased by a factor of 10–2000, whereas D120S is by far the least active mutant.

The activity trend toward nitrocefin is WT > D120N > D120E ≫ D120Q > D120S. The effect on D120N is mostly because of an increased K_m value, whereas D120S displays a drastic decrease on the k_{cat} value. However, the observed SKIE is normal for all mutants, revealing that the rate-limiting step is a proton transfer in all cases. Thus, because k_{cat} (involving a proton transfer) is not significantly affected in D120N, it is quite clear that Asp-120 is not the proton donor in the rate-determining step. This is in agreement with the results from Garrity *et al.* (19) for the MβL L1 from subclass B3 and theoretical calculations on CcrA (28).

Nitrocefin hydrolysis by CcrA and L1 proceeds with accumulation of an anionic intermediate that is favored by the π-delocalized dinitrostyryl moiety unique to this substrate (53, 54). In CcrA and L1, the rate-determining step for nitrocefin hydrolysis is the protonation of the anionic intermediate. Mutation of Asp-120 in these enzymes still gives rise to a normal solvent kinetic isotope effect for nitrocefin hydrolysis, in agreement with our data on Asp-120 BcII mutants. However, because the mechanism of nitrocefin hydrolysis is poised by the stabilization of the anionic intermediate, we also measured the solvent kinetic isotope effect in the hydrolysis of cefotaxime, a clinically useful cephalosporin. Kinetic evidence (55), recently supported by theoretical calculations (28), suggests that cefotaxime hydrolysis by dinuclear B1 MβLs takes place in a single-step reaction, *i.e.* without tetrahedral or anionic intermediate accumulation.

For cefotaxime hydrolysis, the activity trend is WT BcII > D120E > D120N > D120Q ≫ D120S. In all cases k_{cat} is reduced, and in D120S, the poor activity is due both to a low k_{cat} and a high K_m values. The SKIE observed for WT BcII and for all the Asp-120 mutants is similar to that observed for nitrocefin hydrolysis. This allows us to conclude that the observed SKIE is a general effect, and not a peculiarity of nitrocefin.

D120E BcII is the most active mutant against cefotaxime and imipenem. A Glu residue in this position may act as a metal ligand (despite altering the position of Zn2), as a general base, or proton donor and may also be involved in a hydrogen bond network as the native enzyme. The observed activity ratios between D120E and D120Q (which ranges only from 1 to 30) are even lower than those between WT BcII (D120) and D120N. Because both cases entail the replacement of an acidic function by an isosteric amide group, we can definitely discard the possibility that residue 120 is the proton donor in the rate-limiting step. In fact, both mutants D120E and D120Q display almost the same catalytic efficiency toward penicillin G and imipenem. Although Glu-120 and Gln-120 may position Zn2 in a similar manner, Glu-120 is a stronger ligand perhaps explaining why this is the more active of the two mutants.

From the mechanistic point of view, β-lactam hydrolysis can be dissected into two steps (see Scheme 1); the nucleophilic attack to the lactam carbonyl group, and the C–N bond scission, which can occur simultaneously with protonation of the bridging nitrogen atom. So far, no evidence of accumulation of the tetrahedral intermediate formed in the first step has been found in any studied MβL (in contrast with the situation met for serine-β-lactamases). In addition, all mechanistic studies in B1, B2, and B3 have revealed normal solvent kinetic isotope effects ($^{D}k_{cat} > 1$), suggesting that the rate-determining step involves a proton transfer (18, 21, 35, 54). At the same time, this allows us to discard the possibility that the nucleophilic attack of a metal-bound water is rate-limiting, because it should give rise to an inverse isotope effect ($^{D}k_{cat} < 1$). This picture clearly suggests that the nucleophilic attack is fast enough so that it is not possible to distinguish kinetically the two steps (28, 55, 56).

Asp-120 has been proposed to orient and polarize the attacking nucleophile (19, 26, 27, 57). If this were the only mechanistic role of Asp-120, its removal would be expected to slow down significantly the step involving the nucleophilic attack, and we might expect to detect inverse isotope effects. In D120S BcII, the main cause of the poor catalytic efficiency is a 400–800-fold decrease in k_{cat}, which implies an increase in the activation energy of ~4 kcal/mol. But even for this mutant, the rate-determining step also involves a proton transfer, as in WT BcII and in the other mutants herein described. This suggests that nucleophile activation is not the major role of Asp-120 even if (as suggested by Crowder and co-workers (19)) the effect cannot be neglected.

In an attempt to better discern the role of Asp-120, we performed a detailed structural study of the least active mutant, D120S. UV-visible and EPR spectroscopy of Co(II)-substituted D120S reveals that this enzyme is able to accommodate a dinuclear center. This is confirmed by the crystal structure of Zn(II) D120S. In this structure, the coordination geometry of the Zn1 site is preserved, except for a larger Zn1-Wat-1 distance. This is in agreement with the absorption spectroscopy data in the Co(II)-substituted mutants, which reveal minor perturbations in the *d-d* bands attributed to the Co(II) ion in the 3H site. The position of Zn2 is modified by the absence of Asp-120, and the metal ion becomes more tightly bound to Cys-221 and His-263, moving away from Zn1 and binding an additional solvent molecule to complete its coordination sphere (Fig. 4). Thus, the major changes in the active site in this mutant are limited to the Zn2 site. These changes are also accompanied by a different orientation of the side chain of Lys-224 that (together with Zn2) has been implicated in substrate binding by interaction with the carboxylate moiety conserved in all β-lactam antibiotics (10, 11, 13, 18).

The low catalytic efficiency of D120S BcII is also because of a 5–10-fold increase in K_m values for all tested substrates. Lys-224 is involved in an H-bond interaction with Wat-2 in D120S BcII and might interact less efficiently with the substrate, hence making substrate binding less favorable. In addition, Zn2 is shifted farther from Zn1. Thus, if the main anchoring point for substrate binding is provided by Zn2 and Lys-224, any bound

substrate would be incorrectly positioned with respect to the nucleophile coming from the Zn1 site. This provides a structural basis for the observed effects on the k_{cat} and K_m values in D120S BcII. These results are in agreement with those from Crowder and co-workers (19), because the same mutation on L1 gave rise to a mono-Zn(II) enzyme unable to bind substrates. B3 lactamases lack Lys-224, thus Zn2 is expected to represent the main substrate-binding element for MβLs of this subclass (15). If so, Zn2 plays a similar role in this respect in B1 and B3 enzymes.

Recent crystallographic studies have reported the trapping of hydrolyzed products by CphA (a B2 MβL) (16) and L1 (a B3 MβL) (58). In both cases, the bridging nitrogen atom of the hydrolyzed β-lactam moiety is bound to Zn2, suggesting a role for this metal ion in polarizing the C–N bond for cleavage after the nucleophilic attack has taken place. Thus, correct positioning of Zn2 should be essential for this step to occur efficiently. This is in line with a recent theoretical study (28) that stresses the role of Zn2 in orienting a water molecule as a proton donor in the rate-determining step of the catalytic mechanism. We have previously shown that Asp-120 becomes protonated at low pH, thus detaching from Zn2 that moves away from its location in the structure at neutral pH, leading to enzyme inactivation (50). Thus, the effect herein observed is similar to the one triggered by Asp-120 protonation at acidic pH. We therefore propose that the main role of Asp-120 is to act as a strong Zn2 ligand defining its location in the active site. Based on a detailed comparison of different B1 lactamase structures, Murphy *et al.* (59) have recently suggested that the precise position of Asp-120 is essential in defining the affinity for Zn2, providing further support to this hypothesis.

The broad substrate spectrum of B1 MβLs is consistent with the finding of a broad and shallow active site that allows binding and hydrolysis of diverse β-lactam compounds. Thus, as already highlighted (6), the substrate binding and catalytic features of these enzymes are determined by the positioning of the two Zn(II) ions in the active site. Asp-120 is a strong metal ligand, and its mutation significantly alters the Zn2 location as we have shown here, resulting in impaired lactamase activity. This proposal is fully consistent with the mutagenesis experiments on other MβLs. Taken together, these results support the idea that the Zn2 site (present in all MβLs) is necessary for maximal catalytic efficiency in this class of enzymes.

Acknowledgment—Roberto Steiner is thanked for helpful discussions on the structure refinement.

REFERENCES

1. Fisher, J. F., Meroueh, S. O., and Mobashery, S. (2005) *Chem. Rev.* **105,** 395–424
2. Wilke, M. S., Lovering, A. L., and Strynadka, N. C. (2005) *Curr. Opin. Microbiol.* **8,** 525–533
3. Page, M. I., and Laws, A. P. (1998) *J. Chem. Soc. Chem. Commun.* **1998,** 1609–1617
4. Strynadka, N. C., Adachi, H., Jensen, S. E., Johns, K., Sielecki, A., Betzel, C., Sutoh, K., and James, M. N. (1992) *Nature* **359,** 700–705
5. Sulton, D., Pagan-Roderiguez, D., Zhou, X., Liu, Y., Hujer, A. M., Bethel, C. R., Helfand, M. S., Thomson, J. M., Anderson, V. E., Buynak, J. D., Ng, L. M., and Bonomo, R. A. (2005) *J. Biol. Chem.* **280,** 35528–35536
6. Crowder, M. W., Spencer, J., and Vila, A. J. (2006) *Acc. Chem. Res.* **39,** 721–728
7. Walsh, T. R., Toleman, M. A., Poirel, L., and Nordmann, P. (2005) *Clin. Microbiol. Rev.* **18,** 306–325
8. Garau, G., Di Guilmi, A. M., and Hall, B. G. (2005) *Antimicrob. Agents Chemother.* **49,** 2778–2784
9. Carfi, A., Pares, S., Duee, E., Galleni, M., Duez, C., Frère, J. M., and Dideberg, O. (1995) *EMBO J.* **14,** 4914–4921
10. Fabiane, S. M., Sohi, M. K., Wan, T., Payne, D. J., Bateson, J. H., Mitchell, T., and Sutton, B. J. (1998) *Biochemistry* **37,** 12404–12411
11. Concha, N., Rasmussen, B. A., Bush, K., and Herzberg, O. (1996) *Structure* **4,** 823–836
12. Garcia-Saez, I., Hopkins, J., Papamicael, C., Franceschini, N., Amicosante, G., Rossolini, G. M., Galleni, M., Frere, J. M., and Dideberg, O. (2003) *J. Biol. Chem.* **278,** 23868–23873
13. Toney, J. H., Hammond, G. G., Fitzgerald, P. M., Sharma, N., Balkovec, J. M., Rouen, G. P., Olson, S. H., Hammond, M. L., Greenlee, M. L., and Gao, Y. D. (2001) *J. Biol. Chem.* **276,** 31913–31918
14. Garcia-Saez, I., Mercuri, P. S., Papamicael, C., Kahn, R., Frere, J. M., Galleni, M., Rossolini, G. M., and Dideberg, O. (2003) *J. Mol. Biol.* **325,** 651–660
15. Ullah, J. H., Walsh, T. R., Taylor, I. A., Emery, D. C., Verma, C. S., Gamblin, S. J., and Spencer, J. (1998) *J. Mol. Biol.* **284,** 125–136
16. Garau, G., Bebrone, C., Anne, C., Galleni, M., Frere, J. M., and Dideberg, O. (2005) *J. Mol. Biol.* **345,** 785–795
17. Seny, D., Prosperi-Meys, C., Bebrone, C., Rossolini, G. M., Page, M. I., Noel, P., Frere, J. M., and Galleni, M. (2002) *Biochem. J.* **363,** 687–696
18. Yanchak, M. P., Taylor, R. A., and Crowder, M. W. (2000) *Biochemistry* **39,** 11330–11339
19. Garrity, J. D., Carenbauer, A. L., Herron, L. R., and Crowder, M. W. (2004) *J. Biol. Chem.* **279,** 920–927
20. Yamaguchi, Y., Kuroki, T., Yasuzawa, H., Higashi, T., Jin, W., Kawanami, A., Yamagata, Y., Arakawa, Y., Goto, M., and Kurosaki, H. (2005) *J. Biol. Chem.* **280,** 20824–20832
21. Bounaga, S., Laws, A. P., Galleni, M., and Page, M. I. (1998) *Biochem. J.* **31,** 703–711
22. Wang, Z., Fast, W., and Benkovic, S. J. (1999) *Biochemistry* **38,** 10013–10023
23. Park, H., Brothers, E. N., and Merz, K. M., Jr. (2005) *J. Am. Chem. Soc.* **127,** 4232–4241
24. Yang, Y., Keeney, D., Tang, X., Canfield, N., and Rasmussen, B. A. (1999) *J. Biol. Chem.* **274,** 15706–15711
25. Xu, D., Xie, D., and Guo, H. (2006) *J. Biol. Chem.* **281,** 8740–8747
26. Rasia, R. M., and Vila, A. J. (2002) *Biochemistry* **41,** 1853–1860
27. Dal Peraro, M., Llarrull, L. I., Rothlisberger, U., Vila, A. J., and Carloni, P. (2004) *J. Am. Chem. Soc.* **126,** 12661–12668
28. Dal Peraro, M., Vila, A. J., Carloni, P., and Klein, M. L. (2007) *J. Am. Chem. Soc.* **129,** 2808–2812
29. Sambrook, J., Fitsch, E. F., and Maniatis, T. (1989) *Molecular Cloning, A Laboratory Manual*, 2nd Ed., Cold Spring Harbor, NY
30. Orellano, E. G., Girardini, J. E., Cricco, J. A., Ceccarelli, E. A., and Vila, A. J. (1998) *Biochemistry* **37,** 10173–10180
31. Cricco, J. A. (2002) *Role of a Cys Residue in the Structure and Function of Metallo-beta-Lactamases,* Ph.D. thesis, University of Rosario, Rosario, Argentina
32. Barik, S. (1996) in *Site-directed Mutagenesis in Vitro by Megaprimer PCR* (Trower, M. K., ed) pp. 203–216, Humana Press Inc., Totowa, NJ
33. Llarrull, L. I., and Calcaterra, N. B. (2001) *Biocell* **25,** 62
34. Paul-Soto, R., Bauer, R., Frère, J. M., Galleni, M., Meyer-Klaucke, W., Nolting, H., Rossolini, G. M., de Seny, D., Hernández Valladares, M., Zeppezauer, M., and Adolph, H. W. (1999) *J. Biol. Chem.* **274,** 13242–13249
35. Fast, W., Wang, Z., and Benkovic, S. J. (2001) *Biochemistry* **40,** 1640–1650
36. Paul-Soto, R., Hernandez Valladares, M., Galleni, M., Bauer, R., Zeppezauer, M., Frere, J. M., and Adolph, H. W. (1998) *FEBS Lett.* **438,** 137–140
37. Bennett, B., Benson, N., McEwan, A. G., and Bray, R. C. (1994) *Eur. J. Biochem.* **225,** 321–331
38. Leslie, A. G. W. (1992) *Joint CCP4 and ESF-EAMBC Newsl. on Protein*

Crystallogr. **26,** 27–33
39. Collaborative Computational Project Number 4 (1994) *Acta Crystallogr. Sect. D Biol. Crystallogr.* **50,** 760–763
40. Brunger, A. T., Adams, P. D., Clore, G. M., DeLano, W. L., Gros, P., Grosse-Kunstleve, R. W., Jiang, J. S., Kuszewski, J., Nilges, M., Pannu, N. S., Read, R. J., Rice, L. M., Simonson, T., and Warren, G. L. (1998) *Acta Crystallogr. Sect. D Biol. Crystallogr.* **54,** 905–921
41. Emsley, P., and Cowtan, K. (2004) *Acta Crystallogr. Sect. D Biol. Crystallogr.* **60,** 2126–2132
42. Painter, J., and Merritt, E. A. (2006) *Acta Crystallogr. Sect. D Biol. Crystallogr.* **62,** 439–450
43. Painter, J., and Merritt, E. A. (2006) *J. Appl. Crystallogr.* **39,** 109–111
44. Vaguine, A. A., Richelle, J., and Wodak, S. J. (1999) *Acta Crystallogr. Sect. D Biol. Crystallogr.* **55,** 191–205
45. Laskowski, R. A., Mac Arthur, M. W., Moss, D. S., and Thornton, J. M. (1993) *J. Appl. Crystallogr.* **26,** 283–291
46. Lovell, S. C., Davis, I. W., Arendall, W. B., III, de Bakker, P. I., Word, J. M., Prisant, M. G., Richardson, J. S., and Richardson, D. C. (2003) *Proteins* **50,** 437–450
47. Crawford, P. A., Yang, K. W., Sharma, N., Bennett, B., and Crowder, M. W. (2005) *Biochemistry* **44,** 5168–5176
48. Bienvenue, D. L., Gilner, D. M., Davis, R. S., Bennett, B., and Holz, R. C. (2003) *Biochemistry* **42,** 10756–10763
49. Breece, R. M., Costello, A., Bennett, B., Sigdel, T. K., Matthews, M. L., Tierney, D. L., and Crowder, M. W. (2005) *J. Biol. Chem.* **280,** 11074–11081
50. Davies, A. M., Rasia, R. M., Vila, A. J., Sutton, B. J., and Fabiane, S. M. (2005) *Biochemistry* **44,** 4841–4849
51. Prosperi-Meys, C., de Seny, D., Llabres, G., Galleni, M., and Lamotte-Brasseur, J. (2002) *Cell. Mol. Life Sci.* **59,** 2136–2143
52. Dal Peraro, M., Vila, A. J., and Carloni, P. (2003) *Inorg. Chem.* **42,** 4245–4247
53. Wang, Z., Fast, W., and Benkovic, S. J. (1998) *J. Am. Chem. Soc.* **120,** 10788–10789
54. McManus-Muñoz, S., and Crowder, M. W. (1999) *Biochemistry* **38,** 1547–1553
55. Rasia, R. M., and Vila, A. J. (2004) *J. Biol. Chem.* **279,** 26046–26051
56. Spencer, J., Clarke, A. R., and Walsh, T. R. (2001) *J. Biol. Chem.* **276,** 33638–33644
57. Dal Peraro, M., Vila, A. J., and Carloni, P. (2002) *J. Biol. Inorg. Chem.* **7,** 704–712
58. Spencer, J., Read, J., Sessions, R. B., Howell, S., Blackburn, G. M., and Gamblin, S. J. (2005) *J. Am. Chem. Soc.* **127,** 14439–14444
59. Murphy, T. A., Catto, L. E., Halford, S. E., Hadfield, A. T., Minor, W., Walsh, T. R., and Spencer, J. (2006) *J. Mol. Biol.* **357,** 890–903

Asp-120 Locates Zn2 for Optimal Metallo-β-lactamase Activity

Leticia I. Llarrull, Stella M. Fabiane, Jason M. Kowalski, Brian Bennett, Brian J. Sutton and Alejandro J. Vila

J. Biol. Chem. 2007, 282:18276-18285.
doi: 10.1074/jbc.M700742200 originally published online April 10, 2007
